

# AdvDreamer Unveils: Are Vision-Language Models Truly Ready for Real-World 3D Variations?

Shouwei Ruan<sup>1†</sup>, Hanqing Liu<sup>1†</sup>, Yao Huang<sup>1</sup>, Xiaoqi Wang<sup>1</sup>, Caixin Kang<sup>1</sup>,  
Hang Su<sup>2</sup>, Yinpeng Dong<sup>2</sup>, Xingxing Wei<sup>1\*</sup>

<sup>1</sup>Institute of Artificial Intelligence, Beihang University

<sup>2</sup> Dept. of Comp. Sci. and Tech., Institute for AI, Tsinghua-Bosch Joint ML Center,  
THBI Lab, BNRist Center, Tsinghua University

{shouweiruan, hqliu, y-huang, zy2342127, caixinkang, xxwei}@buaa.edu.cn, {suhangss, dongyinpeng}@tsinghua.edu.cn

## Abstract

Vision Language Models (VLMs) have exhibited remarkable generalization capabilities, yet their robustness in dynamic real-world scenarios remains largely unexplored. To systematically evaluate VLMs' robustness to real-world 3D variations, we propose **AdvDreamer**, the first framework that generates physically reproducible adversarial 3D transformation (Adv-3DT) samples from single-view images. AdvDreamer integrates advanced generative techniques with two key innovations and aims to characterize the worst-case distributions of 3D variations from natural images. To ensure adversarial effectiveness and method generality, we introduce an **Inverse Semantic Probability Objective** that executes adversarial optimization on fundamental vision-text alignment spaces, which can be generalizable across different VLM architectures and downstream tasks. To mitigate the distribution discrepancy between generated and real-world samples while maintaining physical reproducibility, we design a **Naturalness Reward Model** that provides regularization feedback during adversarial optimization, preventing convergence towards hallucinated and unnatural elements. Leveraging AdvDreamer, we establish **MM3DTBench**, the first VQA dataset for benchmarking VLMs' 3D variations robustness. Extensive evaluations on representative VLMs with diverse architectures highlight that 3D variations in the real world may pose severe threats to model performance across various tasks.

## 1. Introduction

Recently, Vision-Language Models (VLMs) [7, 13, 33, 34] have demonstrated remarkable capabilities in bridging visual perception and natural language understanding.

\*Corresponding author.

† Equal contribution.



Figure 1. **Exposing 3D Variation Vulnerabilities in VLMs.** AdvDreamer can generate adversarial 3D transformations (Adv-3DT) samples from single-view natural observation. These samples are physically reproducible through real-world object manipulations, highlighting tangible security concerns in VLM deployments.

Through large-scale image-text pre-training followed by fine-grained instruction tuning [29, 34], these models effectively tackle a wide range of visual-centric tasks, including instruction-based image recognition [42, 48, 58], visual question answering [3, 29, 33, 34], and visual reasoning [9, 10]. Due to their strong generalizability and impressive zero-shot capability, VLMs are increasingly deployed in various safety-critical applications, particularly in autonomous driving [49, 56] and robotic systems [23, 57].

Despite extensive studies validating VLMs' resilience against various distribution shifts (e.g., style variations [2, 60], image corruptions [2], and adversarial perturbations [16, 59, 62]), these investigations primarily focus on 2D perturbations in the digital domain, overlooking a critical challenge in **real-world deployment**: the 3D variations. As VLMs increasingly integrated into dynamic, physical environments, their ability to handle 3D transformations becomes crucial, raising a fundamental question: **Do current VLMs truly possess sufficient robustness to handle distri-**

### *bution shifts arising from real-world 3D variations?*

To systematically evaluate VLMs’ robustness under 3D variations, accurately characterizing real-world Adversarial 3D Transformation (Adv-3DT) examples is crucial. However, this task faces three fundamental challenges: **1) Scene-Prior Scarcity.** Existing approaches heavily rely on explicit 3D representations [4, 21, 37] or multi-view observations [18, 45] to capture worst-case 3D variations through optimization-based methods. However, such rich prior information is rarely available in most real-world scenarios, where typically only a few observations are accessible. This practical constraint naturally motivates our exploration of a zero-shot manner for generating Adv-3DT samples. **2) Distribution Discrepancy.** Current methods struggle to generate Adv-3DT samples that preserve visual fidelity and contextual coherence. Methods utilizing handcrafted 3D assets [4, 21] often suffer from noticeable texture discrepancies with real-world scenarios, while neural reconstruction-based approaches [18, 45] leveraging NeRF [39] or 3DGS [25] either operate in isolated object settings or struggle with complex backgrounds. These limitations result in samples that deviate from natural data distributions, undermining the reliability of robustness evaluations. **3) Generalizable Requirements.** Traditional methods [4, 18] usually involve task-specific objectives with end-to-end optimization, limiting their applicability across diverse VLM architectures and tasks. Thus, a universal optimization method with task-agnostic objectives is essential.

To address these challenges, we propose **AdvDreamer**, a novel framework for capturing real-world Adv-3DT samples with task generalizability. In AdvDreamer, we design an innovative generative pipeline that enables controllable 3D transformations of individual natural images in a zero-shot manner. This design directly tackles the scarcity of scene priors by introducing generative 3D priors, and lays the foundation for further adversarial optimization.

To effectively identify the worst-case 3D transformations, AdvDreamer formulates rigid 3D transformations as an adversarial attack, capturing their underlying distribution through query-based adversarial optimization. We propose two key innovations to guide this process. **Firstly**, to tackle the challenge of distribution discrepancy and ensure physical reproducibility [18] of Adv-3DT samples, we propose the **Naturalness Reward Model (NRM)**. It leverages DINOv2’s [41] rich visual context feedback to regulate the optimization trajectory, preventing the optimal distribution convergence toward generating unnatural or hallucinatory elements. For NRM training, we assemble a dataset comprising 100K random 3D variations samples, each annotated with naturalness scores by GPT-4o, ensuring alignment with human judgment. **Secondly**, we introduce the **Inverse Semantic Probability (ISP) objective**, designed to minimize the semantic probability between ac-

tual textual descriptions and the generated Adv-3DT samples. It operates solely through the foundational components of VLMs: the vision encoders (e.g. the OpenAI CLIP with ViT-L/14 [42] used in LLaVa [34]). This design drives attack focus on fundamental vision-text alignment spaces rather than model-specific layers or task-specific heads, ensuring AdvDreamer’s generalizability across different VLM architectures and downstream tasks.

Through extensive digital and physical experiments, we demonstrate that Adv-3DT samples generated by AdvDreamer can effectively deceive most advanced VLMs systems, including GPTs. These samples exhibit reliable reproducibility in physical scenarios, as depicted in Fig. 1. In summary, This paper makes the following contributions:

(1) We propose AdvDreamer, a novel framework that generates real-world Adv-3DT samples from a single natural image. It eliminates the dependency on explicit 3D assets and multi-view samples that previous methods relied upon. Based on extensive digital and physical experiments, we systematically reveal, for the first time, the vulnerability of VLMs under extreme 3D variations.

(2) We introduce a Naturalness Reward Model to maintain sample naturalness during optimization, ensuring distribution alignment with real-world images and physical reproducibility, and an Inverse Semantic Probability objective to guarantee the transferability of Adv-3DT samples across different VLM architectures and downstream tasks.

(3) We construct the **Multimodal 3D Transformation VQA Benchmark (MM3DTBench)**, comprising the most challenging Adv-3DT samples generated by AdvDreamer or reproduced from physical environments. We provide a comprehensive evaluation across 13 leading VLMs, detailing their performance and vulnerabilities.

## 2. Related Work

### 2.1. Vision-Language Models

Classic Vision-language models (VLMs) [28, 30, 36, 42] achieve cross-modal alignment through diverse pre-training objectives on large-scale image-text pairs [31, 46]. Recent advances in large language models (LLMs) [52, 53] have inspired new VLM architectures that integrate LLM capabilities via projection layers [33, 34] or specialized modules like Q-Former [29]. Through techniques like instruction tuning [34], current VLMs [13, 33, 34] demonstrate enhanced performance across vision-centric tasks, including visual grounding, question answering, and image captioning, etc. These models also enable intelligent systems for task planning and decision-making [23, 57].

Despite their impressive capabilities [35, 42, 59], concerns persist regarding their robustness and generalization under some corner cases, particularly given their widespread application in safety-critical environments. Re-

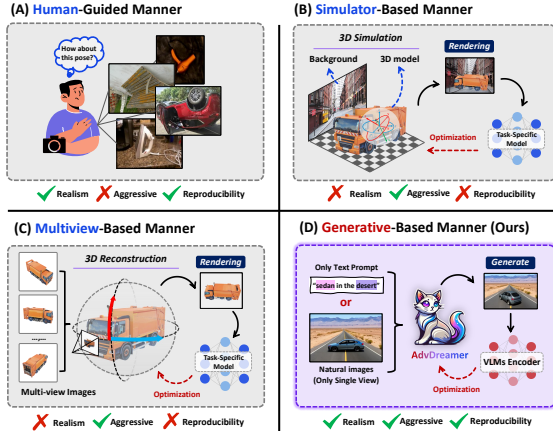


Figure 2. Comparison of paradigms to capture Adv-3DT samples.

cent studies [51] highlight that VLMs still exhibit deficiencies in processing visual details, such as orientation, quantity, and colour, which may be attributed to their visual representations. Moreover, VLMs remain susceptible to  $L_p$ -norm adversarial perturbations [16, 38], with some efforts aiming to enhance their robustness through adversarial fine-tuning techniques [38]. In contrast to previous works, our study specifically investigates VLM robustness against 3D variations, addressing a crucial gap in understanding their reliability for dynamic real-world applications.

## 2.2. Evaluation for 3D Variation Robustness

Robustness & invariance to 3D variations remains a long-standing challenge in computer vision. Evaluating this property typically involves capturing worst-case 3D transformation parameters, such as adversarial poses or viewpoints, to generate challenging samples for assessment. Prior research can be categorized into three approaches (Fig.2). (A) **Human-guided** methods builds benchmarks like ObjectNet[8] and OOD-CV [61] by manually collecting samples with diverse poses and viewpoints. While this approach captures real-world scenarios, it lacks systematic coverage of worst-case examples and incurs high collection costs. (B) **Simulator-based** [4, 21] methods optimize worst-case 3D parameters through differentiable rendering of synthetic objects. However, this approach requires manually designed 3D assets and produces samples with limited realism. (C) **Multi-view-based** methods like ViewFool[18] and GMFool [45] leverage NeRF-based [39] implicit representations to optimize adversarial viewpoints. While avoiding explicit 3D modeling, these methods require multiple views and struggle with background integration.

In contrast, the proposed AdvDreamer adopts a (D) **Generative-based** approach that utilizes robust 3D priors from generative models. Given a single natural image, AdvDreamer synthesizes realistic adversarial 3D transformations in a zero-shot manner, offering a more elegant solution

for evaluating model robustness in real-world scenarios.

## 3. Methodology

### 3.1. Problem Formulation

- **Parametrization of Real-World 3D Variations.** We primarily focus on rigid 3D transformations, *i.e.*, the rotation, translation, and scaling, since they reflect the most typical 3D changes observed in real-world environments. Formally, we define a 6-dimensional vector  $\Theta = \{\alpha, \beta, \gamma, \Delta_x, \Delta_y, s\}$  to uniquely parameterize any arbitrary rigid transformation in 3D space, where  $\alpha, \beta,$  and  $\gamma$  denote the Tait-Bryan angles (yaw, pitch, roll) in the  $z - y - x$  sequence,  $\Delta_x$  and  $\Delta_y$  represent the translation along the  $x$  and  $y$  axes in the  $xy$ -plane, and  $s$  is the uniform scaling factor. To ensure the captured images recognizable by humans [18], we constrain  $\Theta$  within a bounded range  $[\Theta_{\min}, \Theta_{\max}]$ .

- **Optimization Problem.** The goal of AdvDreamer is to find an optimal adversarial distribution  $p(\Theta)$ , ensuring that Adv-3DT sampled from this distribution are both aggressive against VLMs and visually realistic. This can be abstractly formulated as the following optimization problem:

$$p^*(\Theta) = \arg \max_{p(\Theta)} \mathbb{E}_{\Theta \sim p(\Theta)} [\mathcal{L}(\mathcal{G}(\Theta, X))], \quad (1)$$

where  $\mathcal{G}(\Theta, X)$  is a generation process to produce a novel image with the specified transformation  $\Theta$  applied to the original natural image  $X \in \mathbb{R}^3$ . To implement  $\mathcal{G}(\cdot)$ , we designed a pipeline incorporating state-of-the-art generative techniques, which will be detailed in Sec.3.2. The  $\mathcal{L}(\cdot)$  represents the comprehensive loss function guiding the optimization, which assesses the adversarial effectiveness and visual realism of the generated samples. We'll elaborate on the design of each loss component in Sec.3.3 and Sec. 3.4.

Optimizing over the distribution  $p(\Theta)$  rather than a deterministic  $\Theta$  offers two key advantages. 1) As highlighted in [18, 45], learning the underlying distribution enables comprehensive exploration of the 3D variation space, facilitating the identification of the model's vulnerable regions. 2) Given the stochastic nature of the generation, optimizing over a continuous distribution can mitigate the impact of appearance inconsistency, as appearance variations induced by the generation are unlikely to consistently deceive the model without optimizing the adversarial 3D variations [6].

### 3.2. Overview of AdvDreamer

Generating Adv-3DT samples requires accurate 3D scene understanding from 2D images, which has been a long-standing challenge. Fortunately, recent advances in AI generative technologies provide elegant solutions to this problem. As shown in Fig. 3, we design a generation process  $\mathcal{G}(\cdot)$  in a zero-shot manner. In the following contents, we will sequentially detail the critical stages of AdvDreamer.

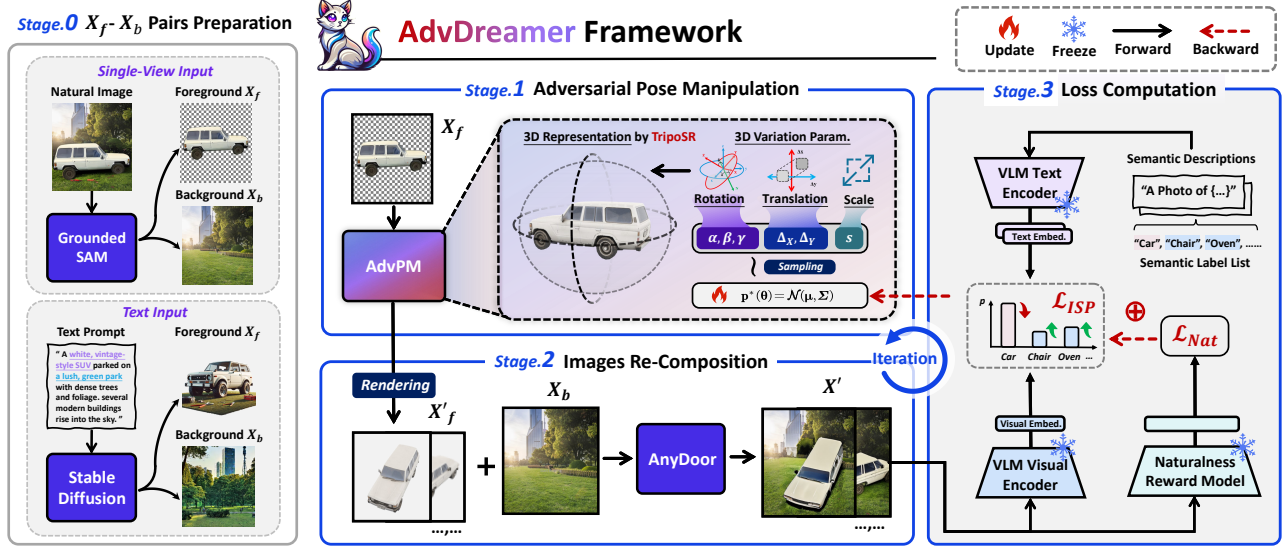


Figure 3. **Overview of the Proposed AdvDreamer Framework.** We first generate foreground-background pairs from the input natural image or text, which are then fed into the optimization process. During each optimization iteration, AdvPM samples transformation parameters from the current adversarial transformation distribution and renders a batch of 3D-transformed foreground samples. We then use Anydoor to composite the transformed foreground samples with the background. These composited samples are used to compute loss, which guides the optimization of the adversarial transformation distribution within AdvPM. This process iterates until convergence.

**Stage0. Foreground-Background Pairs Preparation.** We start by decompose the input image  $X$  into foreground-background pairs  $\{X_f, X_b\}$ . Specifically, we leverage Grounded-SAM [43] to semantically segment the major instance as foreground  $X_f$ , followed by diffusion-based inpainting [15, 44] to obtain a complete background  $X_b$ . This process is denoted as  $\{X_f, X_b\} = \mathcal{F}(X)$ . Additionally, we support directly generating synthetic  $\{X_f, X_b\}$  pairs through Stable-Diffusion [44] to enhance sample diversity.

**Stage1. Adversarial Pose Manipulation.** For each optimization iteration, we employ the proposed Adversarial Pose Manipulator (AdvPM) to transform the foreground  $X_f$  into a batch of  $X'_f$  under  $\Theta$  sampled from current  $p(\Theta)$ . AdvPM leverages the robust priors provided by TripoSR [50], the most advanced Large Reconstruction Model (LRM), to construct single-view-based 3D representations and apply sampled transformations. This process is formulated as  $X'_f = \mathcal{R}_{w_0}(X_f, \Theta)$ , where  $\Theta \sim p(\Theta)$  and  $\mathcal{R}_{w_0}(\cdot)$  denotes TripoSR’s rendering function with weights  $w_0$ .

**Stage2. Images Re-Composition.** Finally, we compose the transformed foreground  $X'_f$  with background  $X_b$  through AnyDoor [12], a diffusion-based composition model that effectively handles shadows and occlusions. This process is defined as  $X' = \mathcal{C}_{w_1}(X'_f, X_b)$ , where  $w_1$  denotes AnyDoor’s weights. Combining *stages 0-2*, the complete generation process can be formally represented as follows:

$$X' = \mathcal{G}(\Theta, X) = \mathcal{C}_{w_1}(\mathcal{R}_{w_0}(X_f, \Theta), X_b), \quad (2)$$

where  $\{X_f, X_b\} = \mathcal{F}(X)$ .

**Stage3. Loss Calculation and Distribution Optimization.**

For each composition sample  $X'$ , we further compute its loss to guide the adversarial distribution update. By iteratively executing *Stages 1-3*, AdvDreamer converges to an optimal distribution  $p^*(\Theta)$ . Sampling from  $p^*(\Theta)$  and applying the generation process yields diverse Adv-3DT samples. Furthermore, the distribution center corresponds to the worst-case Adv-3DT samples.

### 3.3. Inverse Semantic Probability Objective

The Inverse Semantic Probability (ISP) objective aims to minimize the probability that VLMs assign to the ground-truth semantic attributes of Adv-3DT samples. It has two key design considerations. 1) It based solely on the visual encoder  $\mathcal{E}_v$  and text encoder  $\mathcal{E}_t$ , which are fundamental components across modern VLM architectures, ensuring architecture-agnostic applicability. 2), By operating in the vision-text alignment space rather than model-specific layers or task-specific heads, it enables task generalization.

Given a generated sample  $X'$  and a semantic label set  $\mathcal{Y} = \{y_i\}_{i=1}^N$  containing the ground-truth label  $y_i$ , we first compute a semantic similarity vector  $\mathbf{S}$ :

$$\mathbf{S} = \{s_i\}_{i=1}^N, \quad (3)$$

where  $s_i = \cos[\mathcal{E}_v(X'), \mathcal{E}_t(\text{Prompts}(y_i))]$ ,

where  $\cos(\cdot)$  computes cosine similarity and  $\text{Prompts}(\cdot)$  follows the template “a photo of a  $\{y_i\}$ ” in [42]. The vector  $\mathbf{S}$  captures the representation similarities between  $X'$  and each semantic label. We then derive the conditional seman-

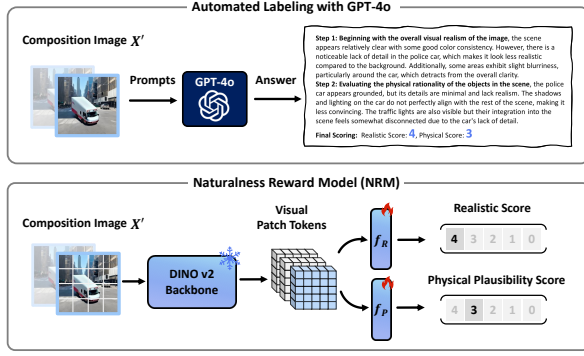


Figure 4. Overview of image naturalness annotation pipeline (Top) and the naturalness reward model (NRM) architecture (Bottom).

tic probability through softmax transformation:

$$p(y_i|X') = \frac{\exp(s_i)}{\sum_{j=1}^N \exp(s_j)}. \quad (4)$$

Then, the  $\mathcal{L}_{\text{IPS}}$  is defined as the negative log-likelihood of the ground-truth’s semantic probability:

$$\mathcal{L}_{\text{IPS}}(X', \mathcal{Y}) = -\log p(y_t|X'). \quad (5)$$

Intuitively,  $\mathcal{L}_{\text{ISP}}$  measures how likely  $X'$  is to be misclassified by comparing its similarity with the ground-truth semantics versus other irrelevant ones. Maximizing this term pushes the adversarial distribution  $p(\Theta)$  towards regions that effectively mislead the model.

### 3.4. Naturalness Reward Model

Despite the 3D priors and realistic image effects provided by generative models, we observe that directly optimizing  $\mathcal{L}_{\text{ISP}}$  often leads to unnatural artifacts, such as shape distortions and physically implausible cases (see Fig. 7). These issues stem from two factors: the generalization limitations of generative models and the inherent high semantic deviation in low-quality samples. To address this challenge, we propose a novel Naturalness Reward Model (NRM) that continuously regularizes  $p(\Theta)$  based on the samples’ naturalness during optimization, preventing convergence to low-quality “pseudo-optimal” regions.

We utilize GPT-4o to create a large-scale training set by automatically annotating the naturalness of 100K carefully selected samples covering various 3D variations. The annotation considers two criteria: visual realism and physical plausibility, each quantified on a 5-point scale. To ensure annotation quality, we conduct manual verification and correct any obvious scoring errors. As shown in Fig. 4, we use DINOv2 [41] as the backbone network  $\mathcal{E}_D$  to extract robust and rich visual features, followed by a dual-stream prediction head for realism and plausibility scoring:

$$\text{Score}_R(X') = f_R(\mathcal{E}_D(X')), \text{Score}_P(X') = f_P(\mathcal{E}_D(X')), \quad (6)$$

### Algorithm 1: Optimization Algorithm of AdvDreamer

---

**Data:** Natural images or text descriptions  $I \in \{X, T\}$ .  
**Result:** Optimal distribution parameters  $\mu^*, \Sigma^*$ .

```

/* Foreground-Background Pairs Preparation */
1  $\{X_f, X_b\} \leftarrow \mathcal{F}(I)$ ;
/* Initialization of distribution parameters */
2  $\mu^0 \leftarrow \mathbf{0}, \Sigma^0 \leftarrow \mathbf{I}$ ;
3 while  $t < t_{\max}$  do
/* Generate a batch of adversarial samples */
4   for  $i = 1 \rightarrow K$  do
5      $\mathbf{z}_i^{t+1} \sim \mathcal{N}(\mu^t, \Sigma^t)$ ;
6      $\Theta_i^{t+1} \leftarrow \mathbf{A} \cdot \tanh(\mathbf{z}_i^{t+1}) + \mathbf{B}$ ;
7      $(X')_i^{t+1} \leftarrow \mathcal{C}_{w_1}(\mathcal{R}_{w_0}(X_f, \Theta_i^{t+1}), X_b)$ ;
/* Calculate loss/fitness value */
8      $\mathcal{L}_i^{t+1} = \mathcal{L}_{\text{IPS}}((X')_i^{t+1}, \mathcal{Y}) + \lambda \cdot \mathcal{L}_{\text{Nat}}((X')_i^{t+1})$ ;
9   end
10  Sorting  $\mathcal{L}_i^{t+1}$  in ascending order;
11  Obtain  $\mu^{t+1}, \Sigma^{t+1}$  by Eq.(10) and (11);
12 end
13  $\mu^* \leftarrow \mu^{t_{\max}}, \Sigma^* \leftarrow \Sigma^{t_{\max}}$ .

```

---

where  $f_R(\cdot)$  and  $f_P(\cdot)$  are implemented as two-layer MLPs trained with cross-entropy loss. Our empirical evaluation demonstrates that NRM achieves high alignment with human assessment (see Appendix.B). Based on NRM’s predictions, we define the naturalness regularization loss as:

$$\mathcal{L}_{\text{Nat}}(X') = -\frac{1}{2}(\text{Score}_R(X') + \text{Score}_P(X')) \quad (7)$$

The  $\mathcal{L}_{\text{Nat}}$  guides the optimization towards adversarial samples that maintain high visual and physical quality.

### 3.5. Query-Based Black-box Optimization

To solve Problem (1), we parameterize the adversarial distribution  $p(\Theta)$  as a *Multivariate Gaussian* form. Specifically, we apply the following random variable approach:

$$\Theta = \mathbf{A} \cdot \tanh(\mathbf{z}) + \mathbf{B}, \text{ where } \mathbf{z} \sim \mathcal{N}(\mu, \Sigma), \quad (8)$$

where  $\mathbf{A} = (\Theta_{\min} - \Theta_{\max})/2$ ,  $\mathbf{B} = (\Theta_{\min} + \Theta_{\max})/2$ ,  $\mathbf{z}$  follows a Gaussian Distribution with mean  $\mu \in \mathbb{R}^6$  and covariance matrix  $\Sigma \in \mathbb{R}^{6 \times 6}$ . Thus, we can rewrite Problem (1) in a more specific form:

$$\arg \max_{\mu, \Sigma} \mathbb{E}_{\mathbf{z} \sim \mathcal{N}(\mu, \Sigma)} [\mathcal{L}_{\text{IPS}}(X', \mathcal{Y}) + \mathcal{L}_{\text{Nat}}(X')], \quad (9)$$

where  $X' = \mathcal{G}(\mathbf{A} \cdot \tanh(\mathbf{z}) + \mathbf{B}, X)$ ,

The solution to this problem typically involves computing the gradient of the loss w.r.t. the distribution parameters  $\mu$  and  $\Sigma$  and updating them via gradient ascent. However, since the forward process involves multiple model components, including the diffusion model, this introduces uncertainty in the gradient propagation path, making optimization using gradient information challenging [47]. Therefore, we adopt the Covariance Matrix Adaptation Evolution Strategy (CMA-ES) [19, 22], an efficient query-based black-box optimizer. At each iteration  $t$ , we: **I**) Sample  $K$  candidates

Table 1. **Zero-shot Classification Accuracy (%) of VLMs Under Adv-3DT Samples Generated from ImageNet and our Synthesis Dataset.** We report the accuracy degradation ( $\downarrow\%$ ) relative to clean samples (**Clean**) under the samples following settings: random 3D transformations (**Random**), sampled transformations from the optimal distribution ( $p^*(\Theta)$ ), and worst-case transformations ( $\Theta$ ).

Target Models	#Params	ImageNet [17]				Synthesis			
		Clean	Random	$p^*(\Theta)$	$\Theta^*$	Clean	Random	$p^*(\Theta)$	$\Theta^*$
OpenCLIP ViT-B/16 [24]	149M	98.0	62.6 ( $\downarrow 35$ )	54.0 ( $\downarrow 44$ )	<b>18.0</b> ( $\downarrow 80$ )	98.0	89.9 ( $\downarrow 8$ )	86.0 ( $\downarrow 12$ )	<b>62.3</b> ( $\downarrow 36$ )
OpenCLIP ViT-L/14 [24]	428M	94.4	61.7 ( $\downarrow 33$ )	50.9 ( $\downarrow 44$ )	<b>15.3</b> ( $\downarrow 79$ )	98.4	89.2 ( $\downarrow 9$ )	83.7 ( $\downarrow 15$ )	<b>62.3</b> ( $\downarrow 36$ )
OpenCLIP ViT-G/14 [24]	2.5B	96.4	63.5 ( $\downarrow 33$ )	53.5 ( $\downarrow 43$ )	<b>18.7</b> ( $\downarrow 78$ )	98.4	89.4 ( $\downarrow 9$ )	86.0 ( $\downarrow 12$ )	<b>62.7</b> ( $\downarrow 36$ )
BLIP ViT-B/16 [28]	583M	83.0	56.0 ( $\downarrow 27$ )	51.3 ( $\downarrow 32$ )	<b>17.3</b> ( $\downarrow 66$ )	92.7	80.4 ( $\downarrow 12$ )	78.6 ( $\downarrow 14$ )	<b>54.7</b> ( $\downarrow 38$ )
BLIP-2 ViT-L/14 FlanT5XL [29]	3.4B	84.0	57.0 ( $\downarrow 27$ )	52.2 ( $\downarrow 32$ )	<b>18.7</b> ( $\downarrow 65$ )	92.7	84.5 ( $\downarrow 8$ )	80.9 ( $\downarrow 12$ )	<b>58.0</b> ( $\downarrow 35$ )
BLIP-2 ViT-G/14 FlanT5XL [29]	4.1B	81.0	55.7 ( $\downarrow 25$ )	49.1 ( $\downarrow 32$ )	<b>15.7</b> ( $\downarrow 65$ )	93.4	85.2 ( $\downarrow 8$ )	82.2 ( $\downarrow 11$ )	<b>61.3</b> ( $\downarrow 32$ )

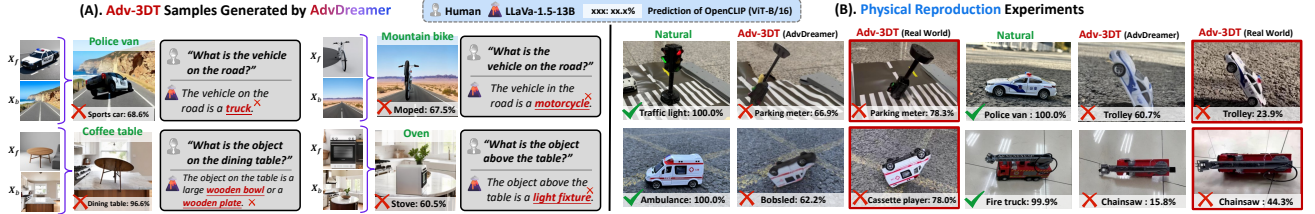


Figure 5. **Visualization of Adv-3DT Samples Generated by AdvDreamer and Their Evaluation Results Across VLMs.** (A) Adv-3DT samples captured in digital environments under synthetic foreground and background. (B) Adv-3DT samples generated from natural photographs and their physical-world reproductions. Each image is annotated with **ground-truth class** in green text.

$\{\mathbf{z}_i^{t+1}\}_{i=1}^k$  from  $\mathcal{N}(\boldsymbol{\mu}^t, \boldsymbol{\Sigma}^t)$ . **2)** Generate corresponding samples  $\{(X')_i^{t+1}\}_{i=1}^k$ . **3)** Update distribution parameters  $\boldsymbol{\mu}^t, \boldsymbol{\Sigma}^t$  using following Strategy:

$$\boldsymbol{\mu}^{t+1} = \sum_{i=1}^k w_i \cdot \mathbf{z}_{(i:k)}^{t+1}, \quad \text{where } \sum_{i=1}^k w_i = 1, \quad (10)$$

$$\boldsymbol{\Sigma}^{t+1} = (1 - \eta_1 - \eta_\mu) \cdot \boldsymbol{\Sigma}^t + \eta_1 \cdot p_\Sigma^{t+1} (p_\Sigma^{t+1})^T + \eta_\mu \cdot \sum_{i=1}^h w_i \cdot \left( \frac{\mathbf{z}_{(i:k)}^{t+1} - \boldsymbol{\mu}^t}{\boldsymbol{\sigma}^t} \right) \left( \frac{\mathbf{z}_{(i:k)}^{t+1} - \boldsymbol{\mu}^t}{\boldsymbol{\sigma}^t} \right)^T, \quad (11)$$

here,  $\mathbf{z}_{(i:k)}$  denotes samples ranked by losses: we first select top-10 samples based on  $\mathcal{L}_{\text{ISP}}$ , then choose the top-k (k=5) with highest  $\mathcal{L}_{\text{Nat}}$  for updates.  $w_i = 1/k$  are importance weights,  $\eta_1$  and  $\eta_\mu$  are learning rates,  $p_\Sigma$  tracks the evolution path, and  $\boldsymbol{\sigma}^t$  is the step size updated via Cumulative Step-size Adaptation (CSA) [22]. Due to space constraints, complete derivations of Eq. (10), (11) and hyperparameter settings are provided in the Appendix.A. We provide the pseudocode for optimization process in algorithms 1.

## 4. Experiments

### 4.1. Experimental Setup

- **Tasks & Datasets.** We evaluate AdvDreamer on three representative vision-language tasks. For **zero-shot image classification**, we use the ImageNet test set [17] and synthetic images generated via Stable Diffusion v2 [44] based on ImageNet categories. For **image captioning**, we leverage the test splits from COCO Caption [11] and No-Caps [1], while **Visual Question Answering (VQA)** on the

VQAv2 [20] test set. For each dataset, we carefully select 150-300 images with clear instance to ensure high-quality Adv-3DT generation. We use ImageNet-1K categories as the semantic label set  $\mathcal{Y}$  for classification tasks, and COCO-80 categories for captioning and VQA tasks.

- **Victim VLMs.** For classification tasks, we target the representative vision-language foundation models: OpenCLIP [14, 24], BLIP [28], and BLIP-2 [29] and consider additional models for the transfer attack. For the remaining tasks, we select the mainstream open-source VLMs (LLaVa series [32, 34], MiniGPT-4 [64], Otter [26], etc.), and most advanced commercial VLMs (GPT-4o and GPT-4o-mini).

- **Methods & Baselines.** In our experiments, we design two attack protocols with AdvDreamer:  $p^*(\Theta)$  represents the average results over 10 Adv-3DT samples randomly sampled from the optimal adversarial distribution, while  $\Theta^*$  indicates the evaluation results using the Adv-3DT sample corresponding to the distribution center. Additionally, we establish two potential baselines: the original natural images without transformation (**Clean**) and the average results over 10 images with random 3D transformations (**Random**).

- **Evaluation Metrics.** For classification tasks, we report **Top-1 accuracy** and its relative drop compared to clean samples. For captioning tasks, beyond common metrics (**CIDEr**, **SPICE**, and **BLEU**), we follow recent works [34, 59, 63] to employ LLM-as-a-judge evaluation. Specifically, we leverage text-only GPT-4 to assess three aspects on a 0-10 scale: semantic accuracy, tone confidence, and overall coherence. These scores sum to a 30-point **GPT-Score**, providing evaluation more aligned with human judgment. For VQA tasks, we adopt **GPT-Acc**, which uses the same LLM-

Table 2. **Performance Degradation ( $\downarrow$ ) of VLMs on Image Captioning and VQA Tasks under Adv-3DT Samples Across Different Metrics.** For BLIP-2 and LLaVa-1.5,  $p^*(\Theta)$  are optimized w.r.t. respective image encoders (i.e., Eva-CLIP and OpenAI CLIP). For other VLMs, transfer attacks are performed using  $p^*(\Theta)$  generated on OpenAI CLIP. Metrics: C-CIDEr, S-SPICE, B-BLUE@4.

Models	#Params	Sample	COCO Caption [11]				NoCaps [1]				VQA-V2 [20]
			C	S	B@4	GPT-Score	C	S	B@4	GPT-Score	GPT-Acc (%)
BLIP-2 [28]	3.4B	Clean	133.4	22.8	36.0	24.7	98.1	14.1	44.1	24.4	53.4
		$p^*(\Theta)$	83.8 ( $\downarrow 50$ )	16.7 ( $\downarrow 6$ )	23.3 ( $\downarrow 13$ )	18.9 ( $\downarrow 6$ )	55.7 ( $\downarrow 42$ )	9.3 ( $\downarrow 5$ )	26.9 ( $\downarrow 17$ )	17.1 ( $\downarrow 7$ )	31.7 ( $\downarrow 22$ )
		$\Theta^*$	<b>72.2</b> ( $\downarrow 61$ )	<b>14.7</b> ( $\downarrow 8$ )	<b>21.5</b> ( $\downarrow 15$ )	<b>17.0</b> ( $\downarrow 8$ )	<b>40.0</b> ( $\downarrow 58$ )	<b>7.3</b> ( $\downarrow 7$ )	<b>22.4</b> ( $\downarrow 22$ )	<b>15.0</b> ( $\downarrow 9$ )	<b>28.0</b> ( $\downarrow 25$ )
LLaVa-1.5 [34]	7B	Clean	126.1	25.7	30.4	25.0	118.7	16.7	50.6	24.7	68.6
		$p^*(\Theta)$	85.8 ( $\downarrow 40$ )	16.7 ( $\downarrow 9$ )	22.9 ( $\downarrow 7$ )	18.9 ( $\downarrow 6$ )	60.0 ( $\downarrow 59$ )	9.7 ( $\downarrow 7$ )	29.6 ( $\downarrow 21$ )	17.4 ( $\downarrow 7$ )	54.3 ( $\downarrow 14$ )
		$\Theta^*$	<b>73.2</b> ( $\downarrow 53$ )	<b>14.4</b> ( $\downarrow 11$ )	<b>20.5</b> ( $\downarrow 10$ )	<b>16.5</b> ( $\downarrow 8$ )	<b>45.8</b> ( $\downarrow 73$ )	<b>8.2</b> ( $\downarrow 9$ )	<b>25.5</b> ( $\downarrow 25$ )	<b>15.6</b> ( $\downarrow 9$ )	<b>53.8</b> ( $\downarrow 15$ )
LLaVa-1.6 [33]	13B	Clean	41.6	11.2	6.9	22.9	30.5	6.9	10.8	22.6	71.2
		$p^*(\Theta)$	21.9 ( $\downarrow 20$ )	6.5 ( $\downarrow 5$ )	5.3 ( $\downarrow 2$ )	16.9 ( $\downarrow 6$ )	13.6 ( $\downarrow 17$ )	4.0 ( $\downarrow 3$ )	6.5 ( $\downarrow 4$ )	15.7 ( $\downarrow 7$ )	53.0 ( $\downarrow 18$ )
		$\Theta^*$	<b>16.7</b> ( $\downarrow 25$ )	<b>5.5</b> ( $\downarrow 6$ )	<b>4.6</b> ( $\downarrow 2$ )	<b>15.4</b> ( $\downarrow 7$ )	<b>10.5</b> ( $\downarrow 20$ )	<b>3.0</b> ( $\downarrow 4$ )	<b>4.3</b> ( $\downarrow 7$ )	<b>13.5</b> ( $\downarrow 9$ )	<b>46.9</b> ( $\downarrow 24$ )
Otter [26]	7B	Clean	127.0	22.6	34.9	24.0	76.4	12.1	29.7	22.5	53.9
		$p^*(\Theta)$	67.9 ( $\downarrow 59$ )	13.8 ( $\downarrow 9$ )	17.8 ( $\downarrow 17$ )	17.2 ( $\downarrow 7$ )	45.4 ( $\downarrow 31$ )	7.6 ( $\downarrow 4$ )	19.2 ( $\downarrow 11$ )	16.2 ( $\downarrow 6$ )	44.9 ( $\downarrow 9$ )
		$\Theta^*$	<b>58.9</b> ( $\downarrow 68$ )	<b>13.0</b> ( $\downarrow 10$ )	<b>17.5</b> ( $\downarrow 17$ )	<b>15.8</b> ( $\downarrow 8$ )	<b>36.0</b> ( $\downarrow 40$ )	<b>6.1</b> ( $\downarrow 6$ )	<b>15.7</b> ( $\downarrow 14$ )	<b>14.6</b> ( $\downarrow 8$ )	<b>42.0</b> ( $\downarrow 12$ )
MiniGPT-4 [64]	7B	Clean	78.5	23.3	23.4	24.0	60.8	17.2	28.5	24.7	51.3
		$p^*(\Theta)$	52.3 ( $\downarrow 26$ )	16.4 ( $\downarrow 7$ )	16.3 ( $\downarrow 7$ )	18.1 ( $\downarrow 6$ )	32.9 ( $\downarrow 28$ )	10.2 ( $\downarrow 7$ )	18.4 ( $\downarrow 10$ )	16.7 ( $\downarrow 8$ )	41.0 ( $\downarrow 10$ )
		$\Theta^*$	<b>42.2</b> ( $\downarrow 36$ )	<b>14.1</b> ( $\downarrow 9$ )	<b>12.9</b> ( $\downarrow 11$ )	<b>16.2</b> ( $\downarrow 8$ )	<b>26.6</b> ( $\downarrow 34$ )	<b>8.3</b> ( $\downarrow 9$ )	<b>14.9</b> ( $\downarrow 14$ )	<b>15.0</b> ( $\downarrow 10$ )	<b>34.3</b> ( $\downarrow 17$ )
GPT-4o-mini [40]	-	Clean	23.7	9.6	3.0	23.3	15.7	5.6	2.9	23.0	68.6
		$p^*(\Theta)$	12.5 ( $\downarrow 11$ )	5.2 ( $\downarrow 4$ )	1.2 ( $\downarrow 2$ )	18.0 ( $\downarrow 5$ )	7.8 ( $\downarrow 8$ )	3.6 ( $\downarrow 2$ )	0.6 ( $\downarrow 2$ )	17.2 ( $\downarrow 6$ )	43.4 ( $\downarrow 25$ )
		$\Theta^*$	<b>9.6</b> ( $\downarrow 14$ )	<b>4.2</b> ( $\downarrow 5$ )	<b>1.6</b> ( $\downarrow 1$ )	<b>16.3</b> ( $\downarrow 7$ )	<b>7.3</b> ( $\downarrow 8$ )	<b>2.9</b> ( $\downarrow 3$ )	<b>0.4</b> ( $\downarrow 3$ )	<b>15.5</b> ( $\downarrow 8$ )	<b>42.7</b> ( $\downarrow 26$ )
GPT-4o [40]	-	Clean	51.2	14.2	9.7	25.0	40.7	10.9	11.7	24.9	75.4
		$p^*(\Theta)$	26.4 ( $\downarrow 25$ )	9.0 ( $\downarrow 5$ )	4.6 ( $\downarrow 5$ )	17.7 ( $\downarrow 7$ )	19.1 ( $\downarrow 22$ )	6.5 ( $\downarrow 4$ )	6.5 ( $\downarrow 5$ )	17.0 ( $\downarrow 8$ )	50.7 ( $\downarrow 25$ )
		$\Theta^*$	<b>20.3</b> ( $\downarrow 31$ )	<b>7.3</b> ( $\downarrow 7$ )	<b>4.7</b> ( $\downarrow 5$ )	<b>16.1</b> ( $\downarrow 9$ )	<b>15.8</b> ( $\downarrow 25$ )	<b>5.5</b> ( $\downarrow 5$ )	<b>5.4</b> ( $\downarrow 6$ )	<b>14.6</b> ( $\downarrow 10$ )	<b>50.3</b> ( $\downarrow 25$ )

Table 3. **Transfer Attack Experiments for Zero-shot Classification Tasks.** We collect Adv-3DT samples optimized based on OpenCLIP (ViT-B/16) and BLIP (ViT-B/16) to evaluate their attack transferability to other VLMs and report the accuracy (%).

Target Model	Clean	OpenCLIP [24]		BLIP [28]	
		$p^*(\Theta)$	$\Theta^*$	$p^*(\Theta)$	$\Theta^*$
ALBEF [27]	65.0	<b>37.2</b> ( $\downarrow 28$ )	27.7 ( $\downarrow 37$ )	<b>40.2</b> ( $\downarrow 25$ )	25.7 ( $\downarrow 39$ )
OpenAI CLIP ViT-B/16 [42]	85.3	48.7 ( $\downarrow 37$ )	29.7 ( $\downarrow 56$ )	52.8 ( $\downarrow 32$ )	31.0 ( $\downarrow 54$ )
OpenCLIP ViT-B/16 [24]	97.7	54.0 ( $\downarrow 44$ )	<b>18.0</b> ( $\downarrow 80$ )	59.3 ( $\downarrow 38$ )	34.7 ( $\downarrow 63$ )
Meta-CLIP ViT-B/16 [55]	91.0	49.3 ( $\downarrow 42$ )	30.0 ( $\downarrow 61$ )	53.8 ( $\downarrow 37$ )	29.7 ( $\downarrow 61$ )
BLIP ViT-B/16 [28]	82.7	48.4 ( $\downarrow 34$ )	30.7 ( $\downarrow 52$ )	<b>51.3</b> ( $\downarrow 31$ )	<b>17.3</b> ( $\downarrow 65$ )
BLIP-2 ViT-L/14 [29]	84.0	50.0 ( $\downarrow 34$ )	32.0 ( $\downarrow 52$ )	52.3 ( $\downarrow 32$ )	27.7 ( $\downarrow 56$ )
SigLIP ViT-B/16 [58]	95.3	55.3 ( $\downarrow 40$ )	34.0 ( $\downarrow 61$ )	59.3 ( $\downarrow 36$ )	34.7 ( $\downarrow 61$ )

based evaluation approach to assess answer correctness. All evaluation prompts are detailed in the Appendix.C.

## 4.2. Research Questions (RQs) and Results

- **RQ1: Do current VLMs exhibit sufficient 3D variations robustness?** *Take-away: “Emphatically not. Current VLMs demonstrate severe vulnerability to worst-case 3D variations, with significant performance degradation across various vision-language tasks.”* As shown in Tab. 1, in zero-shot classification, Adv-3DT samples generated by AdvDreamer significantly compromise VLMs’ performance, causing accuracy drops of up to 80%. This substantially outperforms the Random baseline, validating the effectiveness of our optimization strategy. Notably, samples under  $\Theta^*$  induce more severe performance drops than those from the adversarial distribution  $p^*(\Theta)$ , suggesting the existence of extremely vulnerable points in the transformation space.

This vulnerability extends to more complex downstream tasks. For image captioning (Tab. 3), Adv-3DT samples effectively degrade model performance across all metrics, with nearly 50% reduction in GPT-Score across different

Table 4. **Quantitative Results of Physical Reproduction Experiments.** Acc.-accuracy on ImageNet-1K classification; conf.-average confidence score for ground-truth labels; Acc.1/Acc.2-accuracy on multiple-choice/binary verification VQA tasks.

Sample	Zero-shot Cls. (OpenCLIP-B)		VQA (LLaVa-1.5-7B)	
	Acc.	Conf.	Acc.1	Acc.2
Natural	100.0	0.892	83.3	100.0
Adv-3DT (AdvDreamer)	0.0 ( $\downarrow 100$ )	0.003	25.0 ( $\downarrow 58$ )	25.0 ( $\downarrow 75$ )
Adv-3DT (Physical)	51.3 ( $\downarrow 49$ )	0.413	33.6 ( $\downarrow 50$ )	45.1 ( $\downarrow 55$ )

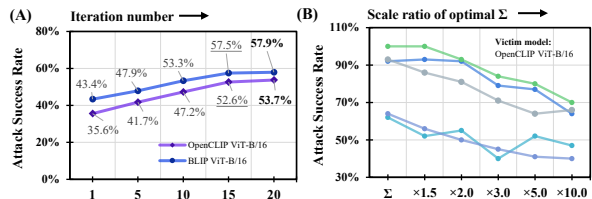


Figure 6. **Ablation Study Results.** Attack success rate (ASR) of Adv-3DT samples w.r.t. (A) different optimization steps and (B) different scaling ratios of the optimal distribution.

VLMs. The consistent degradation in both conventional metrics and human-aligned evaluation (GPT-Score) indicates a fundamental limitation in VLMs’ 3D understanding capabilities. For VQA tasks, even GPT-4o, achieving the highest accuracy (75.4%) on clean samples, exhibits a substantial 25% accuracy drop under Adv-3DT attacks. Fig. 5 presents visualizations of Adv-3DT samples generated by AdvDreamer, with more examples in the Appendix.D.

- **RQ2: Do adversarial 3D variations transfer across different VLMs?** *Take-away: “Yes. Adv-3DT samples demonstrate strong transferability across various VLMs, revealing shared vulnerability region in 3D variation space.”* As

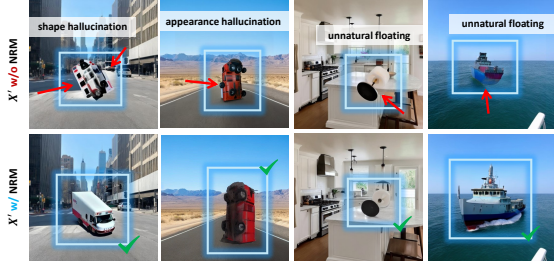


Figure 7. Generated Adv-3DT samples w/ and w/o using NRM.

shown in Tab. 3, we examine transferability using OpenCLIP and BLIP as surrogate models to optimize  $p^*(\Theta)$ , then evaluate six target VLMs with diverse architectures. The transfer attacks maintain strong effectiveness, with performance degradation comparable to direct attacks. Notably,  $p^*(\Theta)$  exhibits smaller transfer gaps than  $\Theta^*$ , suggesting that the learned distribution better captures generalizable vulnerability regions. The transferability also extends to captioning and VQA tasks (Tab. 2). Even when using only OpenCLIP as the surrogate model, Adv-3DT samples effectively compromise all target VLMs except BLIP-2 and LLaVa-1.5, which use their own encoders. We attribute this universal transferability to a fundamental limitation: current pretraining datasets fail to cover diverse 3D variations, resulting in universal performance deficiencies under certain transformation regions.

**- RQ3: Do Adv-3DT samples captured by AdvDreamer reproducible in the physical world?** *Take-away:* “Yes, AdvDreamer successfully identifies physically reproducible adversarial 3D transformations that significantly degrade VLM performance in real-world scenarios. We conduct physical-world experiments on 12 common objects from traffic and household environments. Our protocol consists of three steps: 1) capturing natural-state images of objects, 2) generating Adv-3DT samples using AdvDreamer with OpenCLIP as the surrogate model, and 3) physically reproducing the adversarial 3D transformations captured by AdvDreamer through video recordings. This process yields 3,807 frames of physical Adv-3DT samples.

We evaluate effectiveness through both zero-shot classification and VQA tasks. For VQA, we design two protocols: multiple-choice categorization (Acc.1) and binary verification (Acc.2). As shown in Tab. 4, physically reproduced Adv-3DT samples significantly degrade VLM performance: zero-shot classification accuracy drops to 51.3%, while VQA performance deteriorates to 33.6% (Acc.1) and 45.1% (Acc.2). These results confirm that AdvDreamer successfully captures physically realizable adversarial 3D transformations. However, we observe a moderate performance gap between digital and physical attacks, attributable to the data distribution gap and camera fluctuations. Fig. 5 visualizes representative examples of physical experiments, with additional results provided in the Appendix.D.

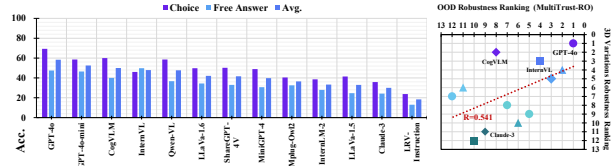


Figure 8. Benchmarking result of VLMs’ 3D variation robustness.

### 4.3. Ablation Studies and Additional Analysis

**- Convergence Analysis.** We analyze the attack success rates (ASR) of  $p^*(\Theta)$  against OpenCLIP (ViT-B/16) and BLIP (ViT-B/16) across different optimization iterations. As shown in Fig. 6 (A), AdvDreamer’s effectiveness consistently improves with more iterations and converges after 15 steps. Based on this observation, we set the iteration step default to 15 throughout our experiments to balance effectiveness and computational efficiency.

**- The Necessity of NRM.** Fig. 7 presents a qualitative comparison between Adv-3DT samples generated with and without NRM. The results demonstrate the effectiveness of NRM’s naturality feedback in enhancing Adv-3DT sample quality and mitigating distribution discrepancy, leading to samples with higher visual quality and better alignment with natural image distributions.

**- Does optimal distribution  $p^*(\Theta)$  effectively characterize the worst-case 3D variations?** We conduct analysis on ImageNet using five random natural images. For each image, we generate 100 Adv-3DT samples by scaling the variance  $\Sigma$  of their  $p^*(\Theta)$  with different ratios. Fig. 6 (B) shows that ASR consistently decreases as the sampling range expands beyond the optimal distribution. This inverse relationship confirms that AdvDreamer successfully identifies the most vulnerable regions in the 3D variation space.

### 4.4. MM3DTBench

We present MM3DTBench for benchmarking the robustness of VLMs to 3D variations. It contains 215 challenging Adv-3DT samples generated by AdvDreamer, along with their physical reproductions. We design two evaluation protocols: a multiple-choice task (**Choice**) and a free-form description task (**Free answer**), with accuracy computed through text-only GPT-4 judgment. More Details of MM3DTBench are provided in the Appendix.E. Our evaluation of 13 representative VLMs reveals robustness gaps. As shown in Fig. 8, even top-performing models (GPT-4o [40], CogVLM [54], and Intern-VL [13]) achieve limited success, while most models struggle with accuracy below 50%. Notably, Claude-3 [5], despite its recognized excellence, only achieves an accuracy of 30.0%. This performance correlates with models’ general out-of-distribution robustness measured by MultiTrust-RO [59], suggesting a fundamental limitation of current VLMs. We encourage the adoption of MM3DTBench in future VLM development to

advance security evaluation in dynamic scenario.

## 5. Conclusion

This paper proposed AdvDreamer, a novel framework for generating physically reproducible and realistic adversarial 3D transformation samples from single-view images. Our comprehensive evaluation revealed critical robustness gaps in existing VLMs, highlighting the urgent need to enhance VLMs' 3D variation perception and understanding capabilities in safety-critical applications. Through MM3DTBench, we established the first benchmark for worst-case 3D variations, aiming to facilitate the development of more robust vision-language systems for real-world deployment.

## References

- [1] Harsh Agrawal, Karan Desai, Yufei Wang, Xinlei Chen, Rishabh Jain, Mark Johnson, Dhruv Batra, Devi Parikh, Stefan Lee, and Peter Anderson. Nocaps: Novel object captioning at scale. In *Proceedings of the IEEE/CVF international conference on computer vision*, pages 8948–8957, 2019. 6, 7
- [2] Haider Al-Tahan, Quentin Garrido, Randall Balestriero, Diane Bouchacourt, Caner Hazirbas, and Mark Ibrahim. Unibench: Visual reasoning requires rethinking vision-language beyond scaling. *arXiv preprint arXiv:2408.04810*, 2024. 1
- [3] Jean-Baptiste Alayrac, Jeff Donahue, Pauline Luc, Antoine Miech, Iain Barr, Yana Hasson, Karel Lenc, Arthur Mensch, Katherine Millican, Malcolm Reynolds, et al. Flamingo: a visual language model for few-shot learning. *Advances in neural information processing systems*, 35:23716–23736, 2022. 1
- [4] Michael A Alcorn, Qi Li, Zhitao Gong, Chengfei Wang, Long Mai, Wei-Shinn Ku, and Anh Nguyen. Strike (with) a pose: Neural networks are easily fooled by strange poses of familiar objects. In *Proceedings of the IEEE/CVF conference on computer vision and pattern recognition*, pages 4845–4854, 2019. 2, 3
- [5] Anthropic. claude-3. <https://www.anthropic.com/claude>, 2024. 8
- [6] Anish Athalye, Logan Engstrom, Andrew Ilyas, and Kevin Kwok. Synthesizing robust adversarial examples. In *International conference on machine learning*, pages 284–293. PMLR, 2018. 3
- [7] Jinze Bai, Shuai Bai, Shusheng Yang, Shijie Wang, Sinan Tan, Peng Wang, Junyang Lin, Chang Zhou, and Jingren Zhou. Qwen-vl: A frontier large vision-language model with versatile abilities. *arXiv preprint arXiv:2308.12966*, 2023. 1
- [8] Andrei Barbu, David Mayo, Julian Alverio, William Luo, Christopher Wang, Dan Gutfreund, Josh Tenenbaum, and Boris Katz. Objectnet: A large-scale bias-controlled dataset for pushing the limits of object recognition models. *Advances in neural information processing systems*, 32, 2019. 3
- [9] Boyuan Chen, Zhuo Xu, Sean Kirmani, Brain Ichter, Dorsa Sadigh, Leonidas Guibas, and Fei Xia. Spatialvlm: Endowing vision-language models with spatial reasoning capabilities. In *Proceedings of the IEEE/CVF Conference on Computer Vision and Pattern Recognition*, pages 14455–14465, 2024. 1
- [10] Liangyu Chen, Bo Li, Sheng Shen, Jingkang Yang, Chunyuan Li, Kurt Keutzer, Trevor Darrell, and Ziwei Liu. Large language models are visual reasoning coordinators. *Advances in Neural Information Processing Systems*, 36, 2024. 1
- [11] Xinlei Chen, Hao Fang, Tsung-Yi Lin, Ramakrishna Vedantam, Saurabh Gupta, Piotr Dollár, and C Lawrence Zitnick. Microsoft coco captions: Data collection and evaluation server. *arXiv preprint arXiv:1504.00325*, 2015. 6, 7
- [12] Xi Chen, Lianghai Huang, Yu Liu, Yujun Shen, Deli Zhao, and Hengshuang Zhao. Anydoor: Zero-shot object-level image customization. In *Proceedings of the IEEE/CVF Conference on Computer Vision and Pattern Recognition*, pages 6593–6602, 2024. 4
- [13] Zhe Chen, Jiannan Wu, Wenhai Wang, Weijie Su, Guo Chen, Sen Xing, Muyan Zhong, Qinglong Zhang, Xizhou Zhu, Lewei Lu, et al. Internvl: Scaling up vision foundation models and aligning for generic visual-linguistic tasks. In *Proceedings of the IEEE/CVF Conference on Computer Vision and Pattern Recognition*, pages 24185–24198, 2024. 1, 2, 8
- [14] Mehdi Cherti, Romain Beaumont, Ross Wightman, Mitchell Wortsman, Gabriel Ilharco, Cade Gordon, Christoph Schuhmann, Ludwig Schmidt, and Jenia Jitsev. Reproducible scaling laws for contrastive language-image learning. In *Proceedings of the IEEE/CVF Conference on Computer Vision and Pattern Recognition*, pages 2818–2829, 2023. 6
- [15] Guillaume Couairon, Jakob Verbeek, Holger Schwenk, and Matthieu Cord. Diffedit: Diffusion-based semantic image editing with mask guidance. In *ICLR 2023 (Eleventh International Conference on Learning Representations)*, 2023. 4
- [16] Xuanming Cui, Alejandro Aparcedo, Young Kyun Jang, and Ser-Nam Lim. On the robustness of large multimodal models against image adversarial attacks. In *Proceedings of the IEEE/CVF Conference on Computer Vision and Pattern Recognition*, pages 24625–24634, 2024. 1, 3
- [17] Jia Deng, Wei Dong, Richard Socher, Li-Jia Li, Kai Li, and Li Fei-Fei. Imagenet: A large-scale hierarchical image database. In *2009 IEEE conference on computer vision and pattern recognition*, pages 248–255. Ieee, 2009. 6
- [18] Yinpeng Dong, Shouwei Ruan, Hang Su, Caixin Kang, Xingxing Wei, and Jun Zhu. Viewfool: Evaluating the robustness of visual recognition to adversarial viewpoints. In *Neural Information Processing Systems (NeurIPS)*, 2022. 2, 3
- [19] Daniel Golovin, Benjamin Solnik, Subhodeep Moitra, Greg Kochanski, John Karro, and David Sculley. Google vizier: A service for black-box optimization. In *Proceedings of the 23rd ACM SIGKDD international conference on knowledge discovery and data mining*, pages 1487–1495, 2017. 5
- [20] Yash Goyal, Tejas Khot, Douglas Summers-Stay, Dhruv Batra, and Devi Parikh. Making the v in vqa matter: Elevating

- the role of image understanding in visual question answering. In *Proceedings of the IEEE conference on computer vision and pattern recognition*, pages 6904–6913, 2017. 6, 7
- [21] Abdullah Hamdi and Bernard Ghanem. Towards analyzing semantic robustness of deep neural networks. In *ECCV*, pages 22–38. Springer, 2020. 2, 3
- [22] Nikolaus Hansen. The cma evolution strategy: A tutorial. *arXiv preprint arXiv:1604.00772*, 2016. 5, 6
- [23] Wenlong Huang, Chen Wang, Ruohan Zhang, Yunzhu Li, Jiajun Wu, and Li Fei-Fei. Voxposer: Composable 3d value maps for robotic manipulation with language models. *arXiv preprint arXiv:2307.05973*, 2023. 1, 2
- [24] Gabriel Ilharco, Mitchell Wortsman, Ross Wightman, Cade Gordon, Nicholas Carlini, Rohan Taori, Achal Dave, Vaishaal Shankar, Hongseok Namkoong, John Miller, Hananeh Hajishirzi, Ali Farhadi, and Ludwig Schmidt. openclip, 2021. 6, 7
- [25] Bernhard Kerbl, Georgios Kopanas, Thomas Leimkühler, and George Drettakis. 3d gaussian splatting for real-time radiance field rendering. *ACM Trans. Graph.*, 42(4):139–1, 2023. 2
- [26] Bo Li, Yuanhan Zhang, Liangyu Chen, Jinghao Wang, Fanyi Pu, Jingkang Yang, Chunyuan Li, and Ziwei Liu. Mimic-it: Multi-modal in-context instruction tuning. *arXiv preprint arXiv:2306.05425*, 2023. 6, 7
- [27] Junnan Li, Ramprasaath Selvaraju, Akhilesh Gotmare, Shafiq Joty, Caiming Xiong, and Steven Chu Hong Hoi. Align before fuse: Vision and language representation learning with momentum distillation. *Advances in neural information processing systems*, 34:9694–9705, 2021. 7
- [28] Junnan Li, Dongxu Li, Caiming Xiong, and Steven Hoi. Blip: Bootstrapping language-image pre-training for unified vision-language understanding and generation. In *International conference on machine learning*, pages 12888–12900. PMLR, 2022. 2, 6, 7
- [29] Junnan Li, Dongxu Li, Silvio Savarese, and Steven Hoi. Blip-2: Bootstrapping language-image pre-training with frozen image encoders and large language models. In *International conference on machine learning*, pages 19730–19742. PMLR, 2023. 1, 2, 6, 7
- [30] Liunian Harold Li, Mark Yatskar, Da Yin, Cho-Jui Hsieh, and Kai-Wei Chang. Visualbert: A simple and performant baseline for vision and language. *arXiv preprint arXiv:1908.03557*, 2019. 2
- [31] Tsung-Yi Lin, Michael Maire, Serge Belongie, James Hays, Pietro Perona, Deva Ramanan, Piotr Dollár, and C Lawrence Zitnick. Microsoft coco: Common objects in context. In *Computer Vision–ECCV 2014: 13th European Conference, Zurich, Switzerland, September 6–12, 2014, Proceedings, Part V 13*, pages 740–755. Springer, 2014. 2
- [32] Haotian Liu, Chunyuan Li, Yuheng Li, and Yong Jae Lee. Improved baselines with visual instruction tuning. In *Proceedings of the IEEE/CVF Conference on Computer Vision and Pattern Recognition*, pages 26296–26306, 2024. 6
- [33] Haotian Liu, Chunyuan Li, Yuheng Li, Bo Li, Yuanhan Zhang, Sheng Shen, and Yong Jae Lee. Llava-next: Improved reasoning, ocr, and world knowledge, 2024. 1, 2, 7
- [34] Haotian Liu, Chunyuan Li, Qingyang Wu, and Yong Jae Lee. Visual instruction tuning. *Advances in neural information processing systems*, 36, 2024. 1, 2, 6, 7
- [35] Yuan Liu, Haodong Duan, Yuanhan Zhang, Bo Li, Songyang Zhang, Wangbo Zhao, Yike Yuan, Jiaqi Wang, Conghui He, Ziwei Liu, et al. Mmbench: Is your multi-modal model an all-around player? In *European Conference on Computer Vision*, pages 216–233. Springer, 2024. 2
- [36] Jiasen Lu, Dhruv Batra, Devi Parikh, and Stefan Lee. Vilbert: Pretraining task-agnostic visiolinguistic representations for vision-and-language tasks. *Advances in neural information processing systems*, 32, 2019. 2
- [37] Spandan Madan, Timothy Henry, Jamell Dozier, Helen Ho, Nishchal Bhandari, Tomotake Sasaki, Frédo Durand, Hanspeter Pfister, and Xavier Boix. When and how do cnns generalize to out-of-distribution category-viewpoint combinations? *arXiv preprint arXiv:2007.08032*, 2020. 2
- [38] Chengzhi Mao, Scott Geng, Junfeng Yang, Xin Wang, and Carl Vondrick. Understanding zero-shot adversarial robustness for large-scale models. *arXiv preprint arXiv:2212.07016*, 2022. 3
- [39] Ben Mildenhall, Pratul P Srinivasan, Matthew Tancik, Jonathan T Barron, Ravi Ramamoorthi, and Ren Ng. Nerf: Representing scenes as neural radiance fields for view synthesis. In *ECCV*, pages 405–421, 2020. 2, 3
- [40] openai. Gpt-4o. <https://openai.com/index/hello-gpt-4o/>, 2024. 7, 8
- [41] Maxime Oquab, Timothée Darcet, Théo Moutakanni, Huy Vo, Marc Szafraniec, Vasil Khalidov, Pierre Fernandez, Daniel Haziza, Francisco Massa, Alaaeldin El-Nouby, et al. Dinov2: Learning robust visual features without supervision. *arXiv preprint arXiv:2304.07193*, 2023. 2, 5
- [42] Alec Radford, Jong Wook Kim, Chris Hallacy, Aditya Ramesh, Gabriel Goh, Sandhini Agarwal, Girish Sastry, Amanda Askell, Pamela Mishkin, Jack Clark, et al. Learning transferable visual models from natural language supervision. In *International conference on machine learning*, pages 8748–8763. PMLR, 2021. 1, 2, 4, 7
- [43] Tianhe Ren, Shilong Liu, Ailing Zeng, Jing Lin, Kunchang Li, He Cao, Jiayu Chen, Xinyu Huang, Yukang Chen, Feng Yan, et al. Grounded sam: Assembling open-world models for diverse visual tasks. *arXiv preprint arXiv:2401.14159*, 2024. 4
- [44] Robin Rombach, Andreas Blattmann, Dominik Lorenz, Patrick Esser, and Björn Ommer. High-resolution image synthesis with latent diffusion models. In *Proceedings of the IEEE/CVF Conference on Computer Vision and Pattern Recognition (CVPR)*, pages 10684–10695, 2022. 4, 6
- [45] Shouwei Ruan, Yinpeng Dong, Hang Su, Ning Chen, and Xingxing Wei. Towards viewpoint-invariant visual recognition via adversarial training. In *ICCV*, pages 1–10, 2023. 2, 3
- [46] Christoph Schuhmann, Romain Beaumont, Richard Vencu, Cade Gordon, Ross Wightman, Mehdi Cherti, Theo Coombes, Aarush Katta, Clayton Mullis, Mitchell Wortsman, et al. Laion-5b: An open large-scale dataset for training next generation image-text models. *Advances in Neural Information Processing Systems*, 35:25278–25294, 2022. 2

- [47] Jiaming Song, Chenlin Meng, and Stefano Ermon. Denoising diffusion implicit models. *arXiv preprint arXiv:2010.02502*, 2020. 5
- [48] Quan Sun, Yuxin Fang, Ledell Wu, Xinlong Wang, and Yue Cao. Eva-clip: Improved training techniques for clip at scale. *arXiv preprint arXiv:2303.15389*, 2023. 1
- [49] Xiaoyu Tian, Junru Gu, Bailin Li, Yicheng Liu, Chenxu Hu, Yang Wang, Kun Zhan, Peng Jia, Xianpeng Lang, and Hang Zhao. Drivevlm: The convergence of autonomous driving and large vision-language models. *arXiv preprint arXiv:2402.12289*, 2024. 1
- [50] Dmitry Tochilkin, David Pankratz, Zexiang Liu, Zixuan Huang, , Adam Letts, Yangguang Li, Ding Liang, Christian Laforte, Varun Jampani, and Yan-Pei Cao. Triposr: Fast 3d object reconstruction from a single image. *arXiv preprint arXiv:2403.02151*, 2024. 4
- [51] Shengbang Tong, Zhuang Liu, Yuexiang Zhai, Yi Ma, Yann LeCun, and Saining Xie. Eyes wide shut? exploring the visual shortcomings of multimodal llms, 2024. 3
- [52] Hugo Touvron, Thibaut Lavril, Gautier Izacard, Xavier Martinet, Marie-Anne Lachaux, Timothée Lacroix, Baptiste Rozière, Naman Goyal, Eric Hambro, Faisal Azhar, et al. Llama: Open and efficient foundation language models. *arXiv preprint arXiv:2302.13971*, 2023. 2
- [53] Hugo Touvron, Louis Martin, Kevin Stone, Peter Albert, Amjad Almahairi, Yasmine Babaei, Nikolay Bashlykov, Soumya Batra, Prajjwal Bhargava, Shruti Bhosale, et al. Llama 2: Open foundation and fine-tuned chat models. *arXiv preprint arXiv:2307.09288*, 2023. 2
- [54] Weihang Wang, Qingsong Lv, Wenmeng Yu, Wenyi Hong, Ji Qi, Yan Wang, Junhui Ji, Zhuoyi Yang, Lei Zhao, Xixuan Song, et al. Cogvlm: Visual expert for pretrained language models. *arXiv preprint arXiv:2311.03079*, 2023. 8
- [55] Hu Xu, Saining Xie, Xiaoqing Tan, Po-Yao Huang, Russell Howes, Vasu Sharma, Shang-Wen Li, Gargi Ghosh, Luke Zettlemoyer, and Christoph Feichtenhofer. Demystifying clip data. In *The Twelfth International Conference on Learning Representations*, 2024. 7
- [56] Zhenhua Xu, Yujia Zhang, Enze Xie, Zhen Zhao, Yong Guo, Kwan-Yee K Wong, Zhenguo Li, and Hengshuang Zhao. Drivegpt4: Interpretable end-to-end autonomous driving via large language model. *IEEE Robotics and Automation Letters*, 2024. 1
- [57] Naoki Yokoyama, Sehoon Ha, Dhruv Batra, Jiuguang Wang, and Bernadette Bucher. Vlfm: Vision-language frontier maps for zero-shot semantic navigation. In *2024 IEEE International Conference on Robotics and Automation (ICRA)*, pages 42–48. IEEE, 2024. 1, 2
- [58] Xiaohua Zhai, Basil Mustafa, Alexander Kolesnikov, and Lucas Beyer. Sigmoid loss for language image pre-training. In *Proceedings of the IEEE/CVF International Conference on Computer Vision*, pages 11975–11986, 2023. 1, 7
- [59] Yichi Zhang, Yao Huang, Yitong Sun, Chang Liu, Zhe Zhao, Zhengwei Fang, Yifan Wang, Huanran Chen, Xiao Yang, Xingxing Wei, Hang Su, Yinpeng Dong, and Jun Zhu. Benchmarking trustworthiness of multimodal large language models: A comprehensive study, 2024. 1, 2, 6, 8
- [60] Yabin Zhang, Wenjie Zhu, Chenhang He, and Lei Zhang. Lapt: Label-driven automated prompt tuning for ood detection with vision-language models. *Proceedings of the european conference on computer vision (ECCV)*, 2024. 1
- [61] Bingchen Zhao, Shaozuo Yu, Wufei Ma, Mingxin Yu, Shenzhao Mei, Angtian Wang, Ju He, Alan Yuille, and Adam Kortylewski. Ood-cv: A benchmark for robustness to out-of-distribution shifts of individual nuisances in natural images. In *European conference on computer vision*, pages 163–180. Springer, 2022. 3
- [62] Yunqing Zhao, Tianyu Pang, Chao Du, Xiao Yang, Chongxuan Li, Ngai-Man Cheung, and Min Lin. On evaluating adversarial robustness of large vision-language models. In *Thirty-seventh Conference on Neural Information Processing Systems*, 2023. 1
- [63] Lianmin Zheng, Wei-Lin Chiang, Ying Sheng, Siyuan Zhuang, Zhanghao Wu, Yonghao Zhuang, Zi Lin, Zhuohan Li, Dacheng Li, Eric Xing, et al. Judging llm-as-a-judge with mt-bench and chatbot arena. *Advances in Neural Information Processing Systems*, 36:46595–46623, 2023. 6
- [64] Deyao Zhu, Jun Chen, Xiaoqian Shen, Xiang Li, and Mohamed Elhoseiny. Minigpt-4: Enhancing vision-language understanding with advanced large language models. *arXiv preprint arXiv:2304.10592*, 2023. 6, 7